Advances in Radiation Oncology (2022) 7, 100928

advances in radiation oncology

www.advancesradonc.org

Scientific Article

Standardizing the Cardiac Radioablation Targeting Workflow: Enabling Semi-Automated Angulation and Segmentation of the Heart According to the American Heart Association Segmented Model

Martijn H. van der Ree, MD,[a] Jorrit Visser, PhD,[b] R. Nils Planken, MD, PhD,[c] Edith M.T. Dieleman, MD,[b] S. Matthijs Boekholdt, MD, PhD,[a] Brian V. Balgobind, MD, PhD,[b] and Pieter G. Postema, MD, PhD[a,*]

[a]Heart Center, Department of Clinical and Experimental Cardiology, Amsterdam UMC, University of Amsterdam, Cardiovascular Sciences, Amsterdam, The Netherlands; [b]Department of Radiation Oncology, Amsterdam UMC, University of Amsterdam, Amsterdam, The Netherlands; [c]Department of Radiology, Amsterdam UMC, University of Amsterdam, Amsterdam, The Netherlands

Received January 11, 2022; accepted February 17, 2022

Abstract

Purpose: Cardiac radioablation has evolved as a potential treatment modality for therapy-refractory ventricular tachycardia. To standardize cardiac radioablation treatments, promote accurate communication and target identification, and to assess toxicity, robust, and reproducible methods for angulation and cardiac segmentation are paramount. In this study, we developed and evaluated a tool for semiautomated angulation and segmentation according to the American Heart Association 17-segment model.

Methods and Materials: The semiautomated angulation and segmentation of the planning-computed tomography (CT) was based on an in-house developed tool requiring placement of only 4 point-markers and a rotation matrix. For angulation, 2 markers defining the cardiac long-axis were placed: at the cardiac apex and at the center of the mitral valve. A rotation matrix was derived that angulates the CT volume, resulting in the cardiac short axis. Segmentation was subsequently performed based on marking the 2 left ventricular hinge points. To evaluate reproducibility, 5 observers independently placed markers in planning CTs of 6 patients.

Results: The root mean square of the standard deviation for the angulation and segmentation marker positions were $\leq$0.5 cm. The 17 segments were subsequently generated and compared between the observers resulting in a median Dice coefficient of 0.8 (interquartile range: 0.70-0.87) and a median of the mean Hausdorff distance of 0.09 cm (interquartile range: 0.05-0.17). The interquartile ranges of Euler angles α and β, determined by the angulation markers, was less than 3 degrees for all patients except one. For the γ angle, determined by the hinge point markers, the interquartile range was up to 12 degrees.

Conclusions: In this study a method for semiautomatic angulation and segmentation of the heart for cardiac radioablation according to the American Heart Association Segmented Model is presented and evaluated. Based on our results we believe that the segmentation

Sources of support: This study was supported with the Dutch Heart Foundation grant 03-003-2021-T061.

Disclosures: none.

The data presented in this study are available on reasonable request from the corresponding author. The data are not publicly available due to privacy reasons.

*Corresponding author: Pieter G. Postema, MD, PhD; E-mail: p.g.postema@amsterdamumc.nl

https://doi.org/10.1016/j.adro.2022.100928

is reproducible and that it can be used to promote communication between radiation oncology and cardiology, enables cardiology-oriented targeting and permits focused toxicity evaluations.

Introduction

Ventricular tachycardia (VT) is a life-threatening malignant ventricular arrhythmia. In patients at high risk for VT, an implantable cardioverter defibrillator is implanted, which can treat ventricular arrhythmias if they occur. To prevent VT, patients are treated with antiarrhythmic medication or invasive catheter ablation.[1] However, VT may still recur despite these treatments, which may have tremendous effect on quality of life, as well as on morbidity and mortality.[2,3]

In recent years, cardiac radioablation (also known as Stereotactic Arrhythmia Radiation therapy and stereotactic ablative radiation therapy) has evolved as a potential (bail out) treatment modality for patients with therapy-refractory VT.[4] The proarrhythmic cardiac region is first determined and delineated, and subsequently "ablated" with a single fraction radiation therapy dose of 25 Gy. Experience with cardiac radioablation is still very limited but steadily growing worldwide due to promising initial efficacy and safety results.[4] Besides the limited experience with cardiac radioablation worldwide and uncertainties about the underlying working mechanisms,[4-6] the workup and workflow for cardiac radioablation are still incompletely defined. This includes defining the proarrhythmic region as this may not be clearly visualized on cardiac imaging. The target for treatment is thus based on aggregating clinical and electro-anatomic information of several modalities such as noninvasive electrophysiology studies and cardiac imaging resulting in interobserver differences in target definition and delineation.[7] An important aspect in the definition of this target is the different anatomic orientation between cardiology-electrophysiology and radiation oncology, and in cardiology the cardiac axes determine nomenclature and deduction, in radiation oncology the standard orthogonal axes are mainly used. As a potential solution for this problem, the use of the American Heart Association (AHA) 17-segment model has previously been proposed as structured approach for the identification and subsequent targeting and treatment of the proarrhythmic regions.[8]

However, radiation therapy planning systems do not yet have implemented tools available to angulate and segment the heart according to this AHA 17-segment model statement.[9] To standardize treatments and to promote accurate communication and identification of the target for cardiac radioablation, a robust and reproducible method for the angulation and generation of the segments is of clear importance. Moreover, also cardiac toxicity of cardiac radioablation might be more easily assessable using cardiac oriented dose-calculations.

Therefore, in this study we developed and evaluated a method for semiautomated angulation and segmentation of the heart according to the AHA 17-segment model for cardiac radioablation.

Methods and Materials

First, we present the methodology for semiautomated angulation and segmentation. Subsequently, we present the methods for the evaluation of this semiautomated method.

Patients and CT scans

Computed tomography (CT) scans of the 6 consecutive participants of the prospective Stereotactic Arrhythmia Radiotherapy in the Netherlands no. 1 (STARNL-1) trial (Netherlands Trial Register: NL7510) were used. These patients were included with therapy refractory VT with recurrences even after (multiple) VT ablations, and high doses of class 1, 2, and 3 antiarrhythmic drugs. For the CT scans, patients were positioned supine using a knee support and with the arms raised over the head using a thorax support (Thorax support, MacroMedics). Patients received intravenous contrast and the 3-dimensional (3D) CT scans were acquired in free breathing with slice thickness 2.5 mm at 120 kVp (Revolution CT, GE Medical Systems).

Study related investigations and treatment were performed after written informed consent and approved by the institutional ethics committee. As follow-up of this trial is ongoing, efficacy and safety results are not part of the present study.

Angulation and segmentation of the heart

Marker placement and angulation

A CT scan acquires axial slices, perpendicular to the long axis of the body (Fig 1A). In cardiology, however, the cardiac planes are widely used. In these cardiac planes, the heart is displayed in planes perpendicular to the cardiac long axis (Fig 1B). The cardiac long axis is defined as the axis that transects the apex and the center of the mitral valve plane.[9] The cardiac planes can be generated from body planes by means of angulation. This angulation can be performed manually,[8] but may also be performed semiautomated.

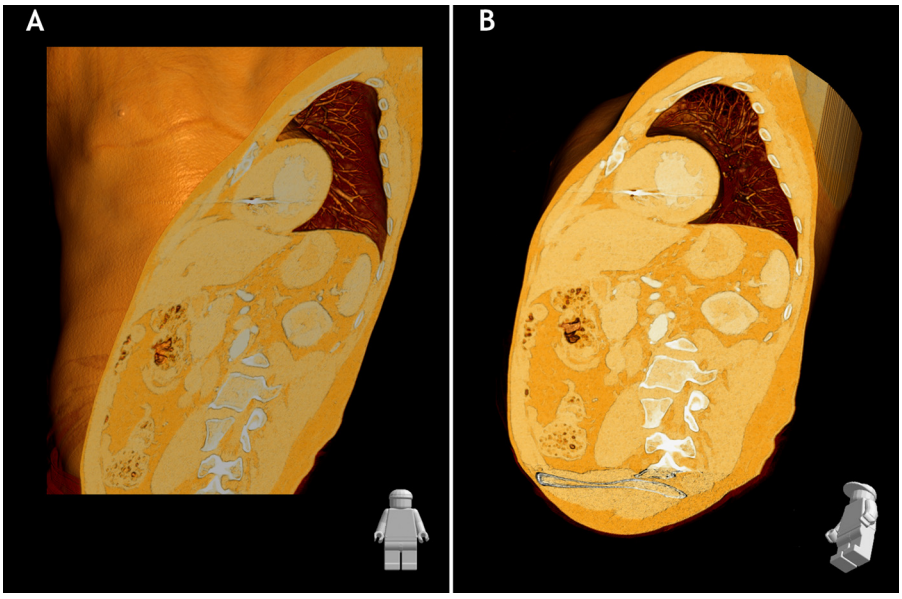

Fig. 1 Volume rendering technique computed tomography images of the chest. (A) Anterior view of the thorax in the coronal plane in which the thorax is transected in the short-axis (SA) plane perpendicular to the cardiac long axis. This long-axis of the heart is defined by the line between the apex and the center of the mitral valve plane (D) by means of angulation the short-axis view of the heart is generated.

For this, CT scans were imported in Velocity (Velocity 4.1, Varian Medical Systems) and 2 markers were positioned in the standard orthogonal planes. In Fig 2, the placement of these markers is described in detail. This was also the instruction that the observers received. The markers are placed at (1) the apex of the heart, and at (2) the center of the mitral valve plane. Subsequently, angulation was performed using an in-house developed tool (described in detail in the text of section 3 of Supplementary E1). Shortly, from the positions of these markers, which define the cardiac long axis, a rotation matrix was derived that angulates the CT volume, resulting in the short axis view of the heart (Fig 3A).

Seventeen segments

The standardized myocardial segmentation into 17 segments has previously been described.[9] After angulation, the LV myocardium was contoured with the use of standard techniques in the short-axis view (Fig 3A). After contouring, the center of the LV was identified in the short-axis view and in the long-axis view (Fig 3A). In the short axis view, 2 markers were set indicating the left ventricular hinge points (ie, the 2 points where the right ventricle and LV fuse; Fig 3B.1). The scan was rotated so that the hinge point markers are perpendicularly above each other (Fig 3B.2). Based on the LV contour and the 2 LV hinge point markers, the coordinate system for the 17 segments was constructed as illustrated in Fig. 3B.2. The LV contour excluding the apical cap, the most inferior part of the left ventricular wall with no visible blood pool, was divided into 3 regions of equal length: the basal, midventricular and apical regions. The 17 segments were subsequently constructed as described in Fig 3 using an in-house developed tool described in detail in the text of section 3 of Supplementary Material E1. In Supplementary Material E2, the 17 segments are shown in all slices of the CT scan of a patient.

Validation of marker placements

To evaluate the reproducibility of the marker placements, 5 observers independently placed markers in the CT scans of the 6 patients (Velocity). The group of observers consisted of a radiologist with cardiac expertise (RP), an imaging cardiologist (SB), a cardiologist-electrophysiologist (PP), an electrophysiology research fellow (MR), and a radiation-oncologist (BB).

Agreement in marker placement

The observers placed the angulation markers in the CT scans. The placement of the ventricular hinge point markers was performed in angulated scans based on the angulation markers of one observer (XX). To determine the agreement on hinge point markers placement alone, the observers placed the ventricular hinge point markers in the same CT slice in the short-axis view of the heart (Fig 3B.1). The effect of ventricular hinge point CT slice selection, as well as hinge point marker placement, was evaluated during the

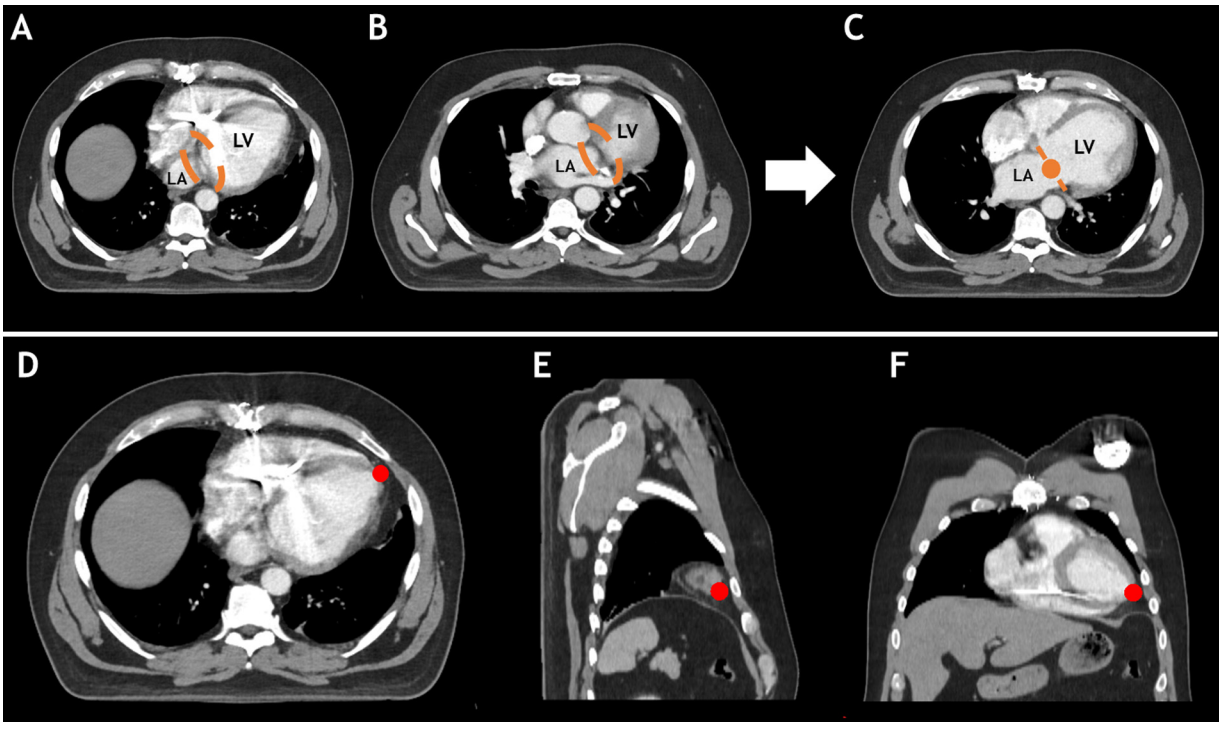

Fig. 2 A computed tomography scan displaying the body in the planes perpendicular to the long axis of the body: axial plane (ABCD), sagittal plane (F), and coronal plane (G). To set a marker in the center of the mitral valve plane, visualize the heart and identify a slice in which there is an "open" connection between the left atrium (LA) and left ventricle (LV). (A) Subsequently identify the inferior border of the mitral valve plane, this is defined as the first slice in which there is no 'open' connection between the LA and the LV (orange circle) (B) repeat this for the superior border of the mitral valve plane (orange circle). (C) Count the number of slices between the superior and inferior borders of the mitral valve plane and divide this number by 2. From inferior or superior, scroll the calculated number of slices up or down to determine the slice exactly in the middle of the mitral valve plane. Set a marker in the center of the mitral valve plane (orange dot). To set the apical marker (red dot), identify the most ventral and caudal part of the heart in the axial (D), sagittal (E), and coronal (F) planes.

comparison of the generated segments. To evaluate observer differences in the position of the angulation- and ventricular hinge point markers, the standard deviations of the X, Y, and Z coordinates of the marker positions were calculated for each patient. For the angulation markers X, Y, and Z refer to the right-to-left, anterior-to-posterior, and caudal-to-cranial direction, respectively, and for the hinge points X and Y are the coordinates in the plane of the short axis view. Differences in the marker positions were summarized by calculating the root mean square (RMS) of the standard deviations over all patients.

Effect of individual marker placements on segmentation

As the segments are generated based on 2 separate sets of markers, the effect on segment generation due to differences in angulation marker placement and subsequent ventricular hinge point CT slice selection and marker placement was evaluated. Based on the placement of the angulation markers of the observers (see the section Agreement in Marker Placement), the scans of the 6 patients were angulated. Thereafter, the observers selected the CT slice visualizing the center of the heart, and the ventricular hinge point markers were placed in their angulated scans. The LV contour was delineated in one angulated scan for each patient. For every patient, this LV contour was propagated to the angulated scans of the other observers. In case the propagation resulted in an LV contour that was not closed at the basal part, this was manually corrected. The 17 segments were generated as described earlier, and for each observer the generated segments were propagated back to the original nonangulated CT scan, together with the LV contour, which enabled comparison between observers. The nonangulated CT scan and all delineations were imported in RayStation (RayStation v8.99, RaySearch). The segments and LV contour were compared by calculating the Dice coefficients and mean and maximum

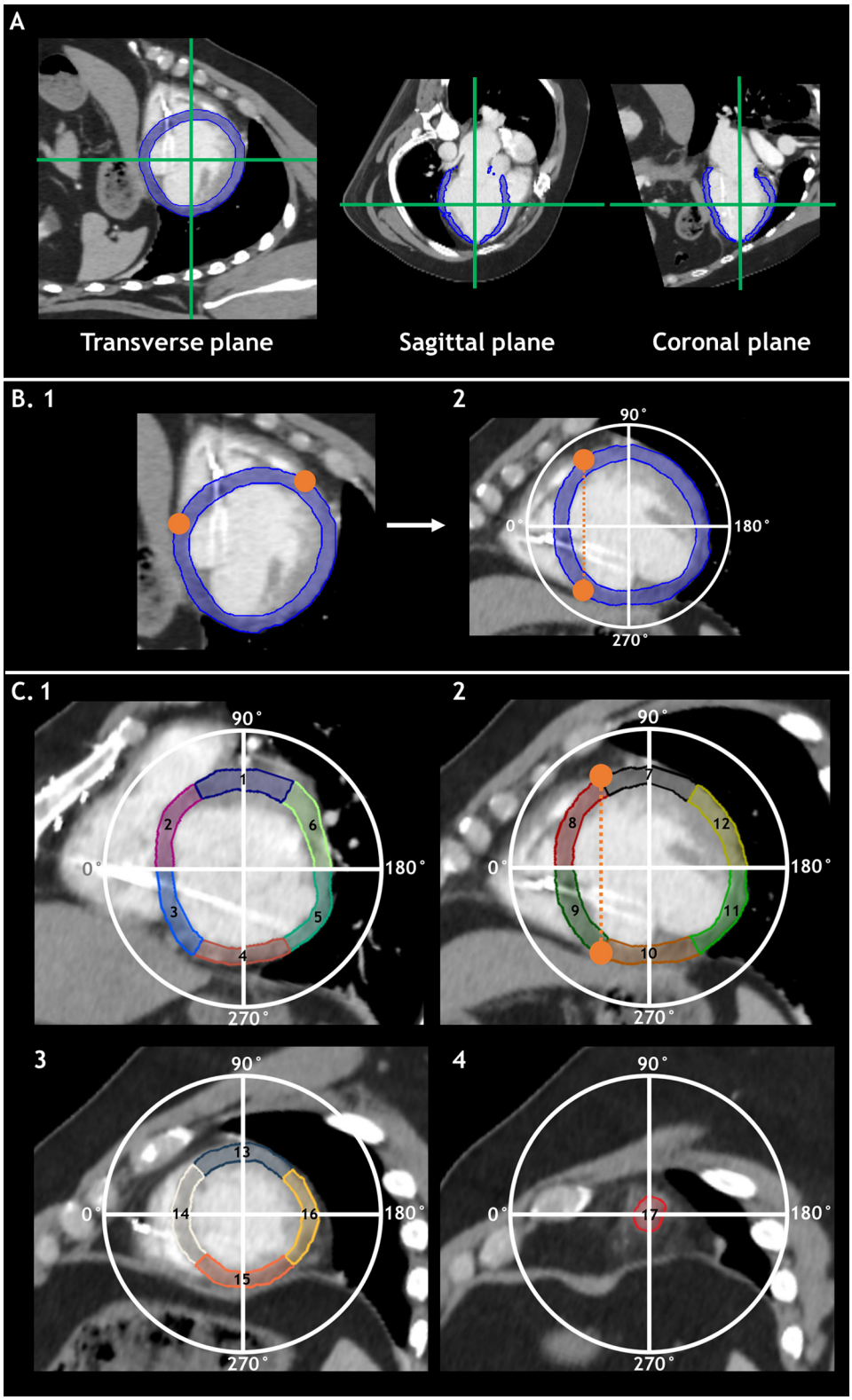

Fig. 3 (A) To set the ventricular hinge point markers, the center of the heart is identified in the transverse plane (short-axis view), sagittal plane and the coronal plane of the angulated scans. (B.1) The 2 ventricular hinge point markers are placed where the LV and RV fuse. (B.2) The scan is rotated so that the hinge point markers are perpendicularly above each other. The coordinate system per slice is constructed based on the center of the LV and the line perpendicular to the ventricular hinge point line (dotted orange line). (C) Illustration of the coordinate system and the generated 17 segments. (C.1) Basal region (segment 1-6): the basal region is the most superior region of the heart above the midventricular region.

Hausdorff distances, which are the distance to agreement, for each combination of observers using a method in the scripting interface of RayStation.[10] A Dice coefficient of 0 indicates no overlap in volumes, and a value of 1 indicates complete overlap. The lower the Hausdorff distance, the smaller the distance between the segments; a Hausdorff distance of 0 indicates complete overlap. To visualize differences, heat maps with percentage agreement per voxel between the observers were generated.

Interobserver variation evaluation by Euler angles and angles between rotation axes

The set of markers for angulation and the set of ventricular hinge point markers on the resulting angulated CT scan together define a rotation matrix. Rotations around a fixed coordinate system can be described using 3 angles, the Euler angles (α, β, and γ). Euler angle α and β are determined by the angulation markers and γ by the hinge point markers. The Euler angles were compared between the observers. The description of the angles, methods and the results are explained in detail in the text and figures of section 1 of Supplementary Material E1. Furthermore, for each combination of 2 observers the difference between the rotation matrices was quantified. This analysis and the results are also described in detail in the text and figures of section 1 of Supplementary Material E1.

Statistical analysis

Statistical analysis of the data was performed with SPSS Statistics (version 26.0, IBM Corporation, Armonk, NY) and using R (R Core Team, 2019. R: A language and environment for statistical computing, R Foundation for Statistical Computing, Vienna, Austria). Distribution of the continuous data was evaluated using histograms and Q-Q plots. In case of normal distribution, a mean ± standard deviation is presented; otherwise the median [interquartile range] is shown.

Results

Agreement in marker placement

The RMS of standard deviation of the marker positions were ≤0.5 cm, indicating good anatomic agreement in marker positions between the observers in (Table 1).

Effect of individual marker placements on segmentation

The propagation of the LV contour to the angulated scans of the different observers caused slight differences in LV contour volumes as indicated by a median Dice coefficient of 0.95 (interquartile range: 0.94-0.96), a median of the mean Hausdorff distance of 0.03 (0.02; 0.03) cm and a median maximum Hausdorff distance of 0.52 (interquartile range: 0.39-0.66) cm. The 17 segments were generated and compared between the observers resulting in a median Dice coefficient of 0.8 (interquartile range: 0.70-0.87), a median of the mean Hausdorff distance of 0.09 (interquartile range: 0.05-0.17) cm and a median maximum Hausdorff distance of 0.66 (interquartile range: 0.43-1 .05) cm. In Table 2, the Dice coefficient and Hausdorff distances are presented, in supplemental Table E1 the results are presented per segment. The results for the basal, midventricular and apical regions were similar by means of Dice indices (0.78-0.83) and median of the mean Hausdorff distances (0.07-0.10 cm). The agreement between the observers for the true apex was lower (Table 2). In Fig 4 the observer agreement is visualized with heat maps indicating the percentage agreement between the observers per voxel for one patient.

Interobserver variation evaluation by Euler angles

The interquartile ranges of Euler angle α and β, determined by the angulation markers, was less than 3 degrees for all patients except one, in which the interquartile

The segments of the basal region comprise of 6 equal parts of 60 degrees. (C.2) Midventricular region (segment 7-12): the midventricular region is the middle region of the heart between the apical and basal region. The segments of the midventricular region also comprise of 6 equal parts of 60 degrees. In orange, the hinge points and the line perpendicular to the hinge points, based on which the coordinate system is constructed, are illustrated. (C.3) Apical region (segment 13-16): The apical region is the most inferior region of the heart above the apical cap. The segments of the apical region comprises of 4 equal parts of 90 degrees. (C.4) Apical cap (segment 17): The apical cap, which is the true apex, comprises the inferior circumferential left ventricular wall until the first slice in which the blood pool is visible. Depending on the myocardium thickness, the apical cap may be comprised of a few slices only. Nomenclature of the segments: 1 = basal anterior; 2 = basal anteroseptal; 3 = basal inferoseptal; 4 = basal inferior; 5 = basal inferolateral; 6 = basal anterolateral; 7 = mid anterior; 8 = mid anteroseptal; 9 = mid inferoseptal; 10 = mid inferior; 11 = mid inferolateral; 12 = mid anterolateral; 13 = apical anterior; 14 = apical septal; 15 = apical inferior; 16 = apical lateral; 17 = Apical cap, which is the true apex.

Table 1 Marker position differences between observers evaluated by the root mean square of the standard deviation

	X (right-left)	Y (anterior-posterior)	Z (caudal-cranial)
Apical marker, RMS of the SD (cm)	0.5	0.4	0.3
Basal marker, RMS of the SD (cm)	0.3	0.2	0.3
Anterior ventricular hinge point, RMS of the SD (cm)	0.5	0.2	n.a.*
Posterior ventricular hinge point, RMS of the SD (cm)	0.2	0.3	n.a.*

Abbreviations: n.a. = not applicable; RMS = root mean square; SD = standard deviation.
* See section "Agreement in Marker Placement" of the Methods. For this analysis, slice selection in the caudal-cranial direction was forced to evaluate only the difference in hinge point marker placement.

range of the β-angle was 7 degrees. For the γ angle, determined by the hinge point markers, the interquartile range was larger and up to 12 degrees. In the Figs A4-6 of Supplementary Material E1, boxplots for the 3 Euler angle are presented per patient. The results for the comparison of the rotation matrices for each combination of 2 observers are also presented in Figs A7-8 of Supplementary Material E1.

Discussion

In this study, a method for semiautomated angulation and segmentation of the heart for cardiac radioablation according to the AHA 17-segment model is presented and evaluated. The results of this study show this semiautomated method is reproducible as indicated by high marker placement agreement and low segment variability between observers. The proposed method and these findings may have important clinical relevance as we will explain below.

Cardiac radioablation is a complex multidisciplinary treatment involving different medical specialties. A cardiac radioablation team usually consists of a cardiologist-electrophysiologist, radiation-oncologist, radiologist, and medical physicist. Every medical specialty involved has its own expertise and herewith routines and workflow approaches. Especially for imaging, differences exist in terms of anatomic orientation. Most medical specialties are used to the anatomic planes that are determined by the long axis of the body. In contrast, in cardiology the cardiac planes that are determined by the long axis of heart are used. To collaborate effectively, uniform communication on the anatomy of the heart and the VT target for cardiac radioablation is of utter importance. For this reason, the 17-segment model has previously been proposed.[8] Previously, angulation from the long axis of the body to the cardiac long axis could be performed by means of several manual rotation steps. After angulation, the 17 segments were manually delineated according to the 17-segment model definitions.[9] Both the manual angulation and segmentation are labor-intensive and efficiency may thus be improved by a semiautomated approach. Also, the manual rotation steps and the subsequent manual segmentation may introduce variability and herewith reduces reproducibility. Consequently, this may result in differences per center, which is undesirable. The clinical effect of this variability in terms of targeting, treatment plans and efficacy and safety has not been explored but any effect in a new and rapidly evolving field such as cardiac radioablation should be prevented when possible. To minimize variability due to manual angulation and segmentation, we present a semiautomated method for both steps. This method is based on the placement of 4 anatomic markers that are well-defined and easy to place for both experts of the cardiac anatomy (ie, cardiac radiologist or imaging cardiologist), as well as by the inexperienced (ie, radiation oncologist). To explain our method for segmentation of the 17 segments we used contrast enhanced 3D-CT scans. The delineated segments can be used to guide the target delineation for cardiac radioablation. After registration

Table 2 Dice coefficients and Hausdorff distances per LV region of the 6 patients

Region	Dice coefficient	Mean Hausdorff distance (cm)	Maximum Hausdorff distance (cm)
LV contour	0.95 [0.94-0.96]	0.03 [0.02-0.03]	0.52 [0.39-0.66]
All segments	0.80 [0.70-0.87]	0.09 [0.05-0.17]	0.66 [0.43-1.05]
Basal	0.78 [0.68-0.84]	0.10 [0.06-0.20]	0.70 [0.52-1.11]
Midventricular	0.80 [0.69-0.87]	0.10 [0.06-0.21]	0.67 [0.45-1.09]
Apical	0.83 [0.74-0.88]	0.07 [0.05-0.13]	0.55 [0.39; 0.99]
True apex	0.70 [0.54-0.78]	0.07 [0.04-0.14]	0.47 [0.21-0.74]

Abbreviations: LV = left ventricle
The results are presented as median [interquartile range].

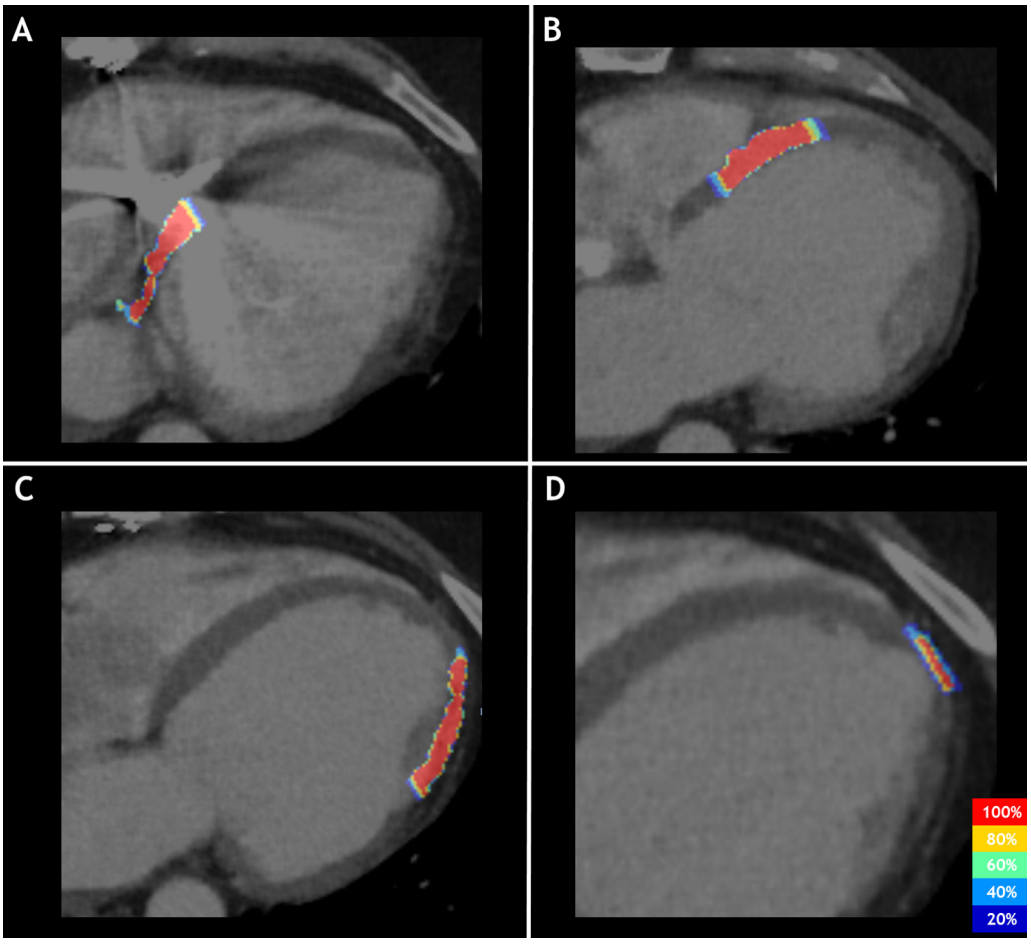

Fig. 4 Heat maps of the generated segments indicating the percentage agreement per voxel between the observers. (A) Segment 3, (B) segment 8, (C) segment 16, and (D) segment 17.

with a phase of the 4-dimensional (4D)-CT the target delineation can be propagated to this phase after which an internal target volume can be created using the other phases of the 4D-CT. Alternatively, if a contrast enhanced 4D-CT is acquired, a phase of the 4D-CT can be used for segmentation of the 17 segments, thereby avoiding the registration error of the registration of the 3D-CT with a phase of the 4D-CT. With regards to the Dice index of the segments, it is important to mention that differences in Dice coefficient already existed due to propagation of the LV contours to the different scan (Dice coefficient of 0.95 [0.94; 0.96]), this should be considered when interpreting the results for the segments. Furthermore, cardiac segments are small volumes, for which slight differences in position result in considerable reduction of the Dice coefficient. Also, in our study the slice thickness of the CT was 2.5 mm and the angulation angles were large, causing inevitable delineation errors when the segments were propagated to the unangulated scans and resulting in a reduced Dice coefficient. For the Euler angles, larger differences were seen for the γ-angle determined by the hinge point markers. This is explained by the fact that the angulation markers determining Euler angle α and β were set in the same CT scan for each observer, and the hinge point markers were set in angulated CT scans that were different for each observer. Although it is important to minimize inter- and intraobserver variability, even in daily clinical practice it will always exist to some degree and remaining observer variability can be incorporated in the planning target volume margin.[10,11] It remains to be elucidated whether the remaining differences after this semiautomated process are an issue of concern for radioablation treatment given the spatiotemporal uncertainties introduced by cardiorespiratory motion. In the future, ECG triggered CT or MRI scans for planning and treatment purposes may improve image quality potentially further reducing intraobserver variability.

It is important to acknowledge that patient's anatomy may differ widely, especially in patients with structural heart disease. For example, in patients qualifying for cardiac radioablation with an ischemic cardiomyopathy, cardiac anatomy may be altered by for example LV aneurysmata.[12] We believe that the effect of these alterations may be minimized using a systematic approach such as in the method proposed. From the patients presented in the manuscript, the sixth patient had an extensive apical aneurysm after an anterior wall myocardial infarction.

This altered anatomy did not result in a larger variability in marker settings. Therefore, even in anatomically more difficult patients, angulation and subsequent segmentation can be reproducibly performed. Unmistakably, the patient's individual anatomy should be considered when determining and delineating the treatment target.

Presently, none of the current treatment planning software systems have implemented tools for angulation and segmentation. Therefore, an in-house developed tool was used which functions outside the planning software systems. It important to mention that this tool was not validated for clinical use and in our center, we only used it as guidance for target delineation and additional research purposes. Still, from the Supplementary Materials, this tool can easily be implemented by other centers. Future commercial treatment planning software packages should incorporate angulation and segmentation tools to further improve cardiac radioablation therapy.

Conclusions

In this study a method for semiautomatic angulation and segmentation of the heart for cardiac radioablation according to the American Heart Association Segmented Model is presented and evaluated. Based on our results we believe that the segmentation is reproducible and that it can be used to promote communication between radiation oncology and cardiology, help guide cardiology-oriented targeting and permits focused toxicity evaluations.

Supplementary materials

Supplementary material associated with this article can be found in the online version at doi:10.1016/j.adro.2022.100928.

References

1. Priori SG, Blomström-Lundqvist C, Mazzanti A, et al. 2015 ESC Guidelines for the management of patients with ventricular arrhythmias and the prevention of sudden cardiac death: The Task Force for the Management of Patients with Ventricular Arrhythmias and the Prevention of Sudden Cardiac Death of the Europe. *Eur Heart J*. 2015;36:2793–2867.
2. Kumar S, Androulakis AFA, Sellal J-M, et al. Multicenter experience with catheter ablation for ventricular tachycardia in lamin A/C cardiomyopathy. *Circ Arrhythm Electrophysiol*. 2016;9: e004357.
3. Tung R, Zimetbaum P, Josephson ME. A critical appraisal of implantable cardioverter-defibrillator therapy for the prevention of sudden cardiac death. *J Am Coll Cardiol*. 2008;52:1111–1121.
4. Ree MH van der, Blanck O, Limpens J, et al. Cardiac radioablation—A systematic review. *Heart Rhythm*. 2020;17:1381–1392.
5. Hohmann S, Deisher AJ, Suzuki A, et al. Left ventricular function after noninvasive cardiac ablation using proton beam therapy in a porcine model. *Hear Rhythm*. 2019;16:1710–1719.
6. Zhang DM, Navara R, Yin T, et al. Cardiac radiotherapy induces electrical conduction reprogramming in the absence of transmural fibrosis. *Nat Commun*. 2021;12:5558.
7. Boda-Heggemann J, Blanck O, Mehrhof F, et al. Interdisciplinary clinical target volume generation for cardiac radioablation: Multicenter benchmarking for the RAdiosurgery for VENtricular TAchycardia (RAVENTA) trial. *Int J Radiat Oncol Biol Phys*. 2021;110:745–756.
8. Brownstein J, Afzal M, Okabe T, et al. Method and Atlas to Enable Targeting for Cardiac Radioablation Employing the American Heart Association Segmented Model. *Int J Radiat Oncol Biol Phys*. 2021;111:178–185.
9. Cerqueira MD, Weissman NJ, Dilsizian V, et al. Standardized myocardial segmentation and nomenclature for tomographic imaging of the heart. *Circulation*. 2002;105:539–542.
10. Vinod SK, Min M, Jameson MG, Holloway LC. A review of interventions to reduce interobserver variability in volume delineation in radiation oncology. *J Med Imaging Radiat Oncol*. 2016;60:393–406.
11. Winter MM, Bernink FJP, Groenink M, et al. Evaluating the systemic right ventricle by CMR: The importance of consistent and reproducible delineation of the cavity. *J Cardiovasc Magn Reson*. 2008;10:1–8.
12. Vallabhajosyula S, Kanwar S, Aung H, et al. Temporal trends and outcomes of left ventricular aneurysm after acute myocardial infarction. *Am J Cardiol*. 2020;133:32–38.